Journal of Hazardous Materials 195 (2011) 115–123

Contents lists available at ScienceDirect

Journal of Hazardous Materials

journal homepage: www.elsevier.com/locate/jhazmat

The oxidative corrosion of carbide inclusions at the surface of uranium metal during exposure to water vapour

T.B. Scott[a,*], J.R. Petherbridge[b], N.J. Harker[a], R.J. Ball[a], P.J. Heard[a], J. Glascott[b], G.C. Allen[a]

[a] Interface Analysis Centre, University of Bristol, 121 St Michaels Hill, Bristol, BS2 8BS, United Kingdom
[b] AWE, Aldermaston, Reading, Berkshire, RG7 4PR, United Kingdom

ARTICLE INFO

Article history:
Received 13 May 2011
Received in revised form 3 August 2011
Accepted 4 August 2011
Available online 10 August 2011

Keywords:
Uranium
Water vapour
Oxidation
Carbide
Inclusions

ABSTRACT

The reaction between uranium and water vapour has been well investigated, however discrepancies exist between the described kinetic laws, pressure dependence of the reaction rate constant and activation energies. Here this problem is looked at by examining the influence of impurities in the form of carbide inclusions on the reaction. Samples of uranium containing 600 ppm carbon were analysed during and after exposure to water vapour at 19 mbar pressure, in an environmental scanning electron microscope (ESEM) system. After water exposure, samples were analysed using secondary ion mass spectrometry (SIMS), focused ion beam (FIB) imaging and sectioning and transmission electron microscopy (TEM) with X-ray diffraction (micro-XRD). The results of the current study indicate that carbide particles on the surface of uranium readily react with water vapour to form voluminous $UO_3{\cdot}xH_2O$ growths at rates significantly faster than that of the metal. The observation may also have implications for previous experimental studies of uranium–water interactions, where the presence of differing levels of undetected carbide may partly account for the discrepancies observed between datasets.

1. Introduction

The interaction between metallic uranium surfaces and water vapour is considered to be most important in regard to the environmental corrosion of the metal. Numerous studies have examined the initial stages of these interactions [1–7]. However, there have been discrepancies in the published data describing kinetic laws, pressure dependence of the reaction rate constant and activation energies. The precise mechanism for uranium corrosion is not entirely clear with different mechanisms proposed arising from the results of the undertaking studies [1–7]. Existing discrepancies in the published data may, in part, be related to differences in the provenance and purity of the metal used by different groups. The reactivity of impurity species such as carbide, may have affected recorded data. This work aims to provide data for an improved understanding of the role of impurity phases in the uranium–water reaction, samples of uranium containing 600 ppm carbon were analysed during and after exposure to water vapour at 19 mbar pressure, in an environmental scanning electron microscope (ESEM). Samples were analysed using secondary ion mass spectrometry (SIMS), focused ion beam (FIB) imaging and sectioning and transmission electron microscopy (TEM) with X-ray diffraction (micro-XRD).

2. Experimental

2.1. Starting materials

The uranium used in the experimental work was cast, depleted uranium containing 600 ppm carbon. Prior analysis of the microstructure before experiment revealed a coarsely grained metal, with grains frequently >100 μm in width with long, relatively straight, low angle (<25°) grain boundaries and occasional sets of well defined crystal twins. Inclusion particles were frequently observed across the metal surface, present as individual particles and conjoined clusters. A surface inclusion number density of 575 per mm^2 (±20) was measured for the metal, with an average inclusion diameter of 5 μm. TEM analysis of a small number of inclusions (removed from a high-carbon uranium sample using FIB) indicated that the inclusions were of mixed UC-UN (carbonitride) composition with FCC crystal structure [8,9]. Hereafter, and for simplicity, these inclusions are referred to as carbides. Examples of carbide particles exposed at the uranium surface are shown in Figs. 1–3 and highlight the occurrence of both individual and clustered 'compound' particles.

2.2. Experimental methods

Uranium sample coupons (15 mm diameter and 1 mm thick), containing 600 ppm carbon were mechanically polished using wetted Buehler SiC grit papers of increasingly fine grade down to

* Corresponding author. Tel.: +44 117 3311176.
E-mail address: t.b.scott@bristol.ac.uk (T.B. Scott).

0304-3894/$ – see front matter.
doi:10.1016/j.jhazmat.2011.08.011

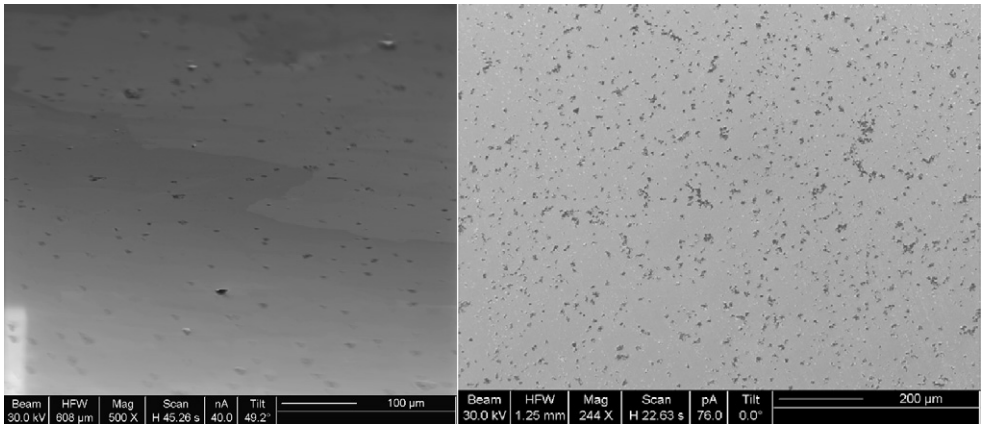

Fig. 1. Secondary electron images of typical electropolished surface regions on the sample metal. Carbide inclusions are highlighted as dark spots 3–8 μm in size.

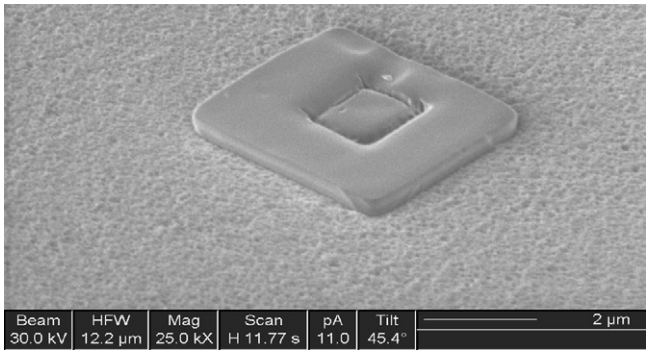

Fig. 2. Secondary electron image of a typical carbide inclusion at the surface of the uranium. The inclusion is obviously zoned, with an outer shell assumed to be uranium carbide, and an inner core of nitride.

4000 grit (equivalent to a 2–3 μm surface finish). Once a satisfactory finish was achieved, each coupon was rinsed and washed using ethanol and electro-polished in a 10:6:6 mixture of ethanol, orthophosphoric acid and ethylene glycol, for a 10 min period. The sample was then dipped in the unbiased electrolyte and rinsed successively with deionised water, ethanol and acetone.

Directly after electro-polishing, the samples were immediately loaded into an Electroscan environmental secondary electron microscope system (ESEM). Water vapour was admitted to the chamber at a constant controlled pressure of 19 mbar, at approximately 20 °C, and the sample surface was imaged at regular intervals for a period of up to one week. Secondary electron images taken from specific areas on the sample surface were compiled, to produce a 'time-lapse' sequence of surface reaction.

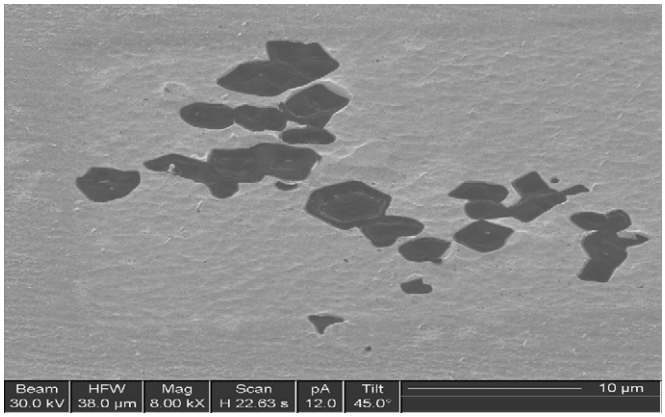

Fig. 3. Secondary electron image of a carbide inclusion cluster at the surface of the uranium, showing numerous compound particles.

The experiment was repeated under identical conditions three times using deionised water as the vapour source and a further three times using a 1:1 mixture of high performance liquid chromatography (HPLC) grade and distilled water as the vapour source. After each experiment the 'reacted' sample coupon was immediately transferred for analysis by FIB imaging and milling with supplementary analysis by SIMS. TEM specimens were also prepared using FIB milling and ex-situ lift-out, as described in Ishitani et al. [10].

Further samples were prepared then exposed to water vapour in the ESEM after using only mechanical polishing (down to a 4000 grit paper) to level the sample surface and remove any oxide present. This experiment was performed in order to determine if sample reactivity differed between preparation methods.

In addition, water exposure was carried out using a separate gas treatment rig to repeat the ESEM experiments. A sample coupon was prepared following the aforementioned procedure (polishing and electropolishing) and loaded into a gasket sealed stainless steel reaction cell of ~30 cm^3 volume. The cell was evacuated to better than 10^{-5} mbar prior to the experiment, and then filled with water vapour to 20 mbar pressure at approximately 22 °C. High purity (<10 ppb O_2, <20 ppb H_2O) argon gas was then immediately added to generate a total system pressure of 1000 mbar and the cell was left for a 24 h period to allow reaction of the metal surface with the water vapour.

2.3. Analytical methods

Both an Electroscan environmental secondary electron microscope system and a FEI FIB Strata 201 focused ion beam system were used to examine the sample morphology and micro-texture. The resolution of each system is dependent on the operating conditions employed, for example, at 30 keV beam energy, the FIB resolution is 500 nm for an operating current above 11 nA and 5–7 nm for a current of 1 pA. Surface images were recorded from the sample at tilt angles of both 0° and 45° to provide complimentary topographical and structural information.

Whilst the ESEM system was primarily used for the water vapour exposure of the metal (rather than imaging), the FIB instrument was used for sample sectioning and preparation of TEM lamella for analysis. TEM images and electron diffraction patterns were obtained using a Philips EM 430 TEM operating at 250 keV beam energy. TEM lamella were mounted on 200 mesh carbon-coated copper grids using an ex situ lift-out method, after FIB preparation. Subsequently a selected area aperture was used to record images

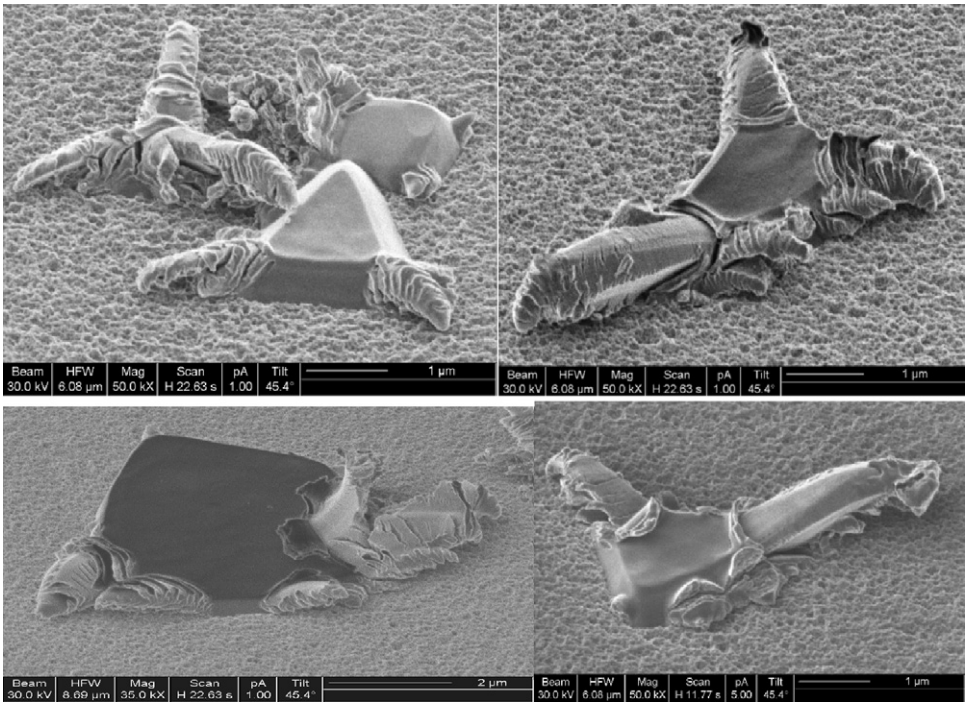

Fig. 4. Secondary electron images of carbide inclusions on the surface of the cast uranium following reaction with water vapour at 20 mbar for 12 h at 20 °C. Horn-like growths were observed to grow at inclusion edges and corners.

and diffraction patterns from specific areas of the TEM lamella to identify the various phases present.

Secondary ion mass spectrometry was performed in negative ion mode using a spectrometer previously constructed at the University of Bristol. The SIMS system employed a focused gallium ion source (FEI electronically variable aperture type) fitted to a Vacuum Generators model 7035 double-focusing magnetic sector mass analyser. During analysis numerous ion maps were recorded at different magnifications with beam currents of 0.5–1 nA. Negative ions and ion clusters corresponding to H^-, C^-, O^-, OH^- and CN^- were mapped from discreet areas of the sample surface, with those for C^- and CN^- being considered to be most characteristic of the carbide inclusions, and

H^-, O^- and OH^- ion clusters considered to best represent the observed surface reaction products. Ion maps for UO^+ and UO_2^+ clusters were also recorded and found to be representative of surface oxides formed on the metal.

3. Results

3.1. Water-sample interactions under ESEM conditions

Upon exposure to water vapour at 20 °C (equivalent to ~85% relative humidity) oxidation of the uranium surfaces was observed. FIB sections cut through the sample material indicated that the oxide on the metal surface thickened considerably over the duration of experiments. After preparatory electropolishing the oxide thickness on the starting material was determined to be 5–20 nm thick (depending on time taken to transfer to the instrument). For comparison, exposure to water vapour for a 24 h period resulted in recorded oxide thicknesses of 90–120 nm, with close to 900 nm thickness after one week.

Whilst the ESEM instrument could not easily detect thickening of oxide on the metal, the oxidative decomposition of the surface carbides was readily apparent, forming voluminous horn-like growths as imaged in the FIB system (Figs. 4 and 5). Corrosion growth was often observed to initiate at the corners and edges of carbide particles and also at boundaries between conjoined particles. Figs. 4 and 5 show a number of representative growth sites, where corrosion product can clearly be seen extending from the carbide to overlie the surrounding surface of the metal. The period of time between the introduction of water vapour and the onset of growth formation was observed to vary from carbide to carbide.

Whilst some carbide particles exhibited corrosion initiation after periods of only minutes, other particles showed no signs of reaction until days into the experiment. Analysis of the samples exposed to water vapour for one week revealed that all visible surface carbide inclusions had undergone some degree of oxidative corrosion and hydrous growth formation. Figs. 6 and 7 display images recorded from defined areas of the sample material before, during and after water vapour exposure in the ESEM system. Fig. 7 clearly illustrates the gradual nature of corrosion growth on a carbide particle. After a period of 6 h water exposure the growth had apparently halted, whilst new ones were formed (and grew) elsewhere on the same carbide particle.

High resolution SEM imaging of reacted carbide particles clearly indicated that the growths initiated beneath a protective surface layer and burst outwards to form a voluminous reaction product (Fig. 5). The protective surface layer on the carbide particles was ascribed to a mixed layer of uranium oxide, uranium hydroxide and free carbon [11] formed during sample preparation and subsequent transfer to the ESEM instrument.

Sections through the growths and parent carbide particles were made with a FIB instrument. Numerous growths were sectioned at different periods of water exposure to chart their relative growth into the carbide particles. An example of a carbide inclusion after 24 h water vapour exposure is shown in Fig. 8. The image shows that the carbide had been completely consumed by a polycrystalline growth of much larger volume, with individual grains ≤100 nm in size. The section also highlights that the oxide covering the metal surface (~87 nm thick) thickens down the margins of the inclusion site. This phenomenon was not observed for other sections where the carbide had not fully decomposed (Fig. 9).

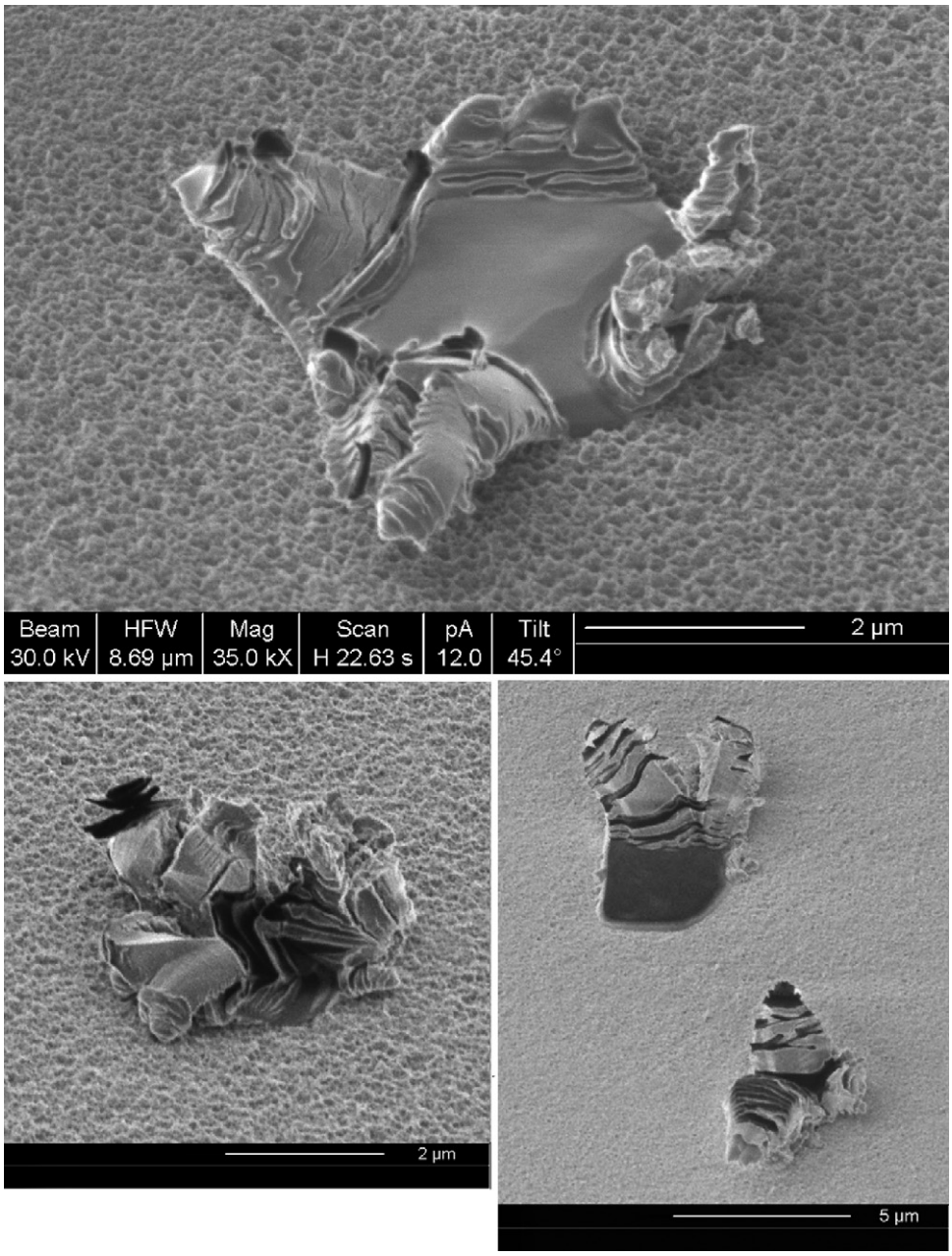

Fig. 5. Secondary electron images of carbide inclusions on the uranium surface following reaction with for 24 h at 20 mbar water vapour pressure and 20 °C. The horn-like precipitates are seen to fragment the surface layer of the carbide during growth.

For each section it was clear that the growth has formed solely from the carbide inclusion and showed no reaction with the surrounding metal (Fig. 9). The cross-sectional shape of the reaction front in the carbides indicated that, once initiated, growth occurred more slowly at the carbide margins than in the bulk of the crystal (Fig. 9). Within the ESEM, growths were observed to stop developing after a period of reaction and it is presumed that either the growth's reaction-front reached an internal chemical boundary within the carbide (possibly zoning from nitride to carbide), which prevented continued reaction.

Concurrent work using combined FIB and electron backscatter diffraction (EBSD) technique has demonstrated that the carbide inclusions present in the metal are single crystals. Additionally SIMS and TEM analysis has shown that these carbide inclusions may also be chemically zoned from nitride to carbide, without a significant change in lattice structure.

In the current experiments, the apparent preference for growth nucleation at the edges and corners of inclusion particles indicates that these parts of the carbide crystals represent low-energy zones for reaction initiation, possibly due to the presence of incomplete (dangling) bonds and/or structural defects at the termination of the crystal lattice.

TEM analysis was performed on a number of lamella produced by FIB ion milling and the structure of the metal, carbide and growth phases was identified using micro-XRD. An example of FIB preparation is shown in Fig. 10. The metal was confirmed as α-uranium and the carbide inclusions were determined to have the expected cubic monocarbide (UC) structure. The growth forming from the carbide inclusions was determined as a nanocrystalline $UO_3{\cdot}xH_2O$ with $0.5 < x < 1.0$. The confirmation of hydrated UO_3 (metaschoepite) as the corrosion product phase provides direct chemical evidence for the reaction of the carbide with water vapour.

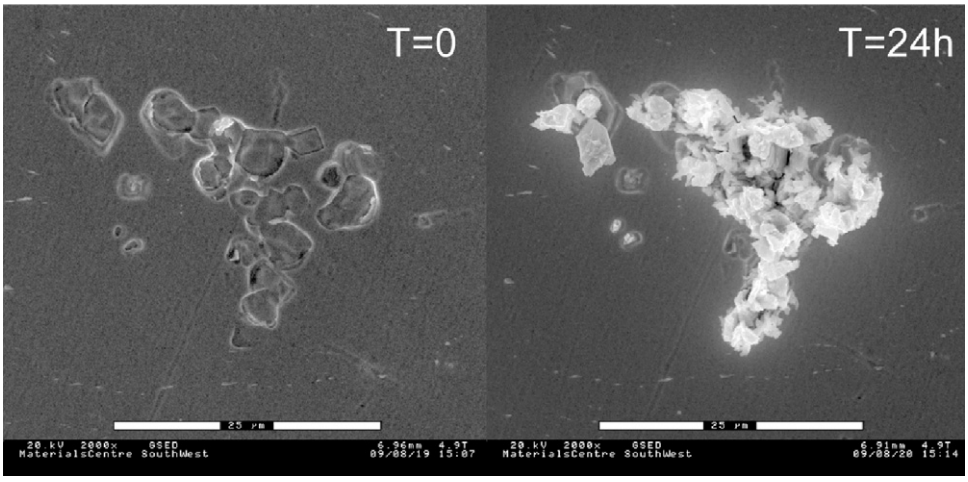

Fig. 6. In situ secondary electron images of carbide inclusions on the uranium surface before and after water vapour exposure for a 24 h period at 19 mbar and 20 °C.

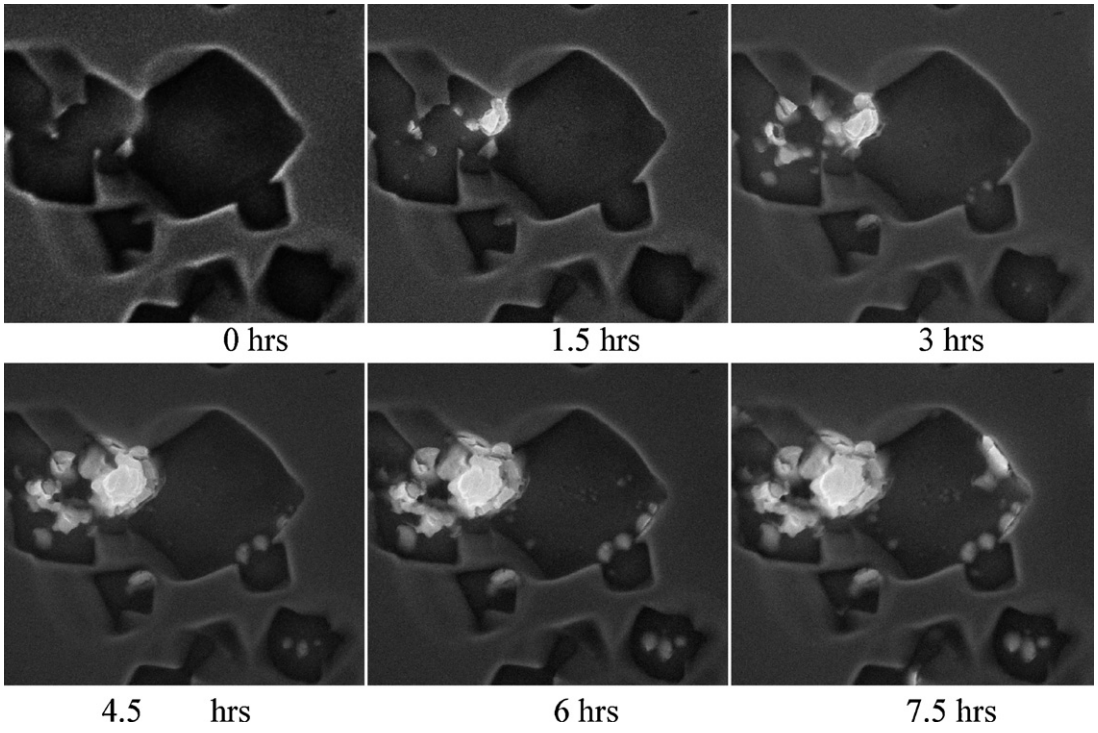

Fig. 7. Secondary electron images of a carbide inclusion cluster on the surface of the cast uranium with increasing lengths of exposure to water vapour at 19 mbar and 20 °C.

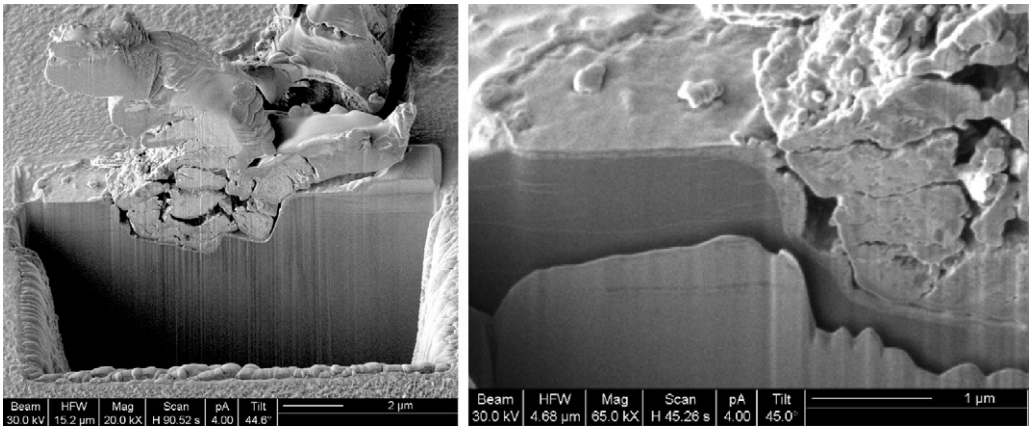

Fig. 8. Secondary electron images of a carbide inclusion cluster on the surface of the cast uranium with increasing lengths of exposure to water vapour at 19 mbar and 20 °C.

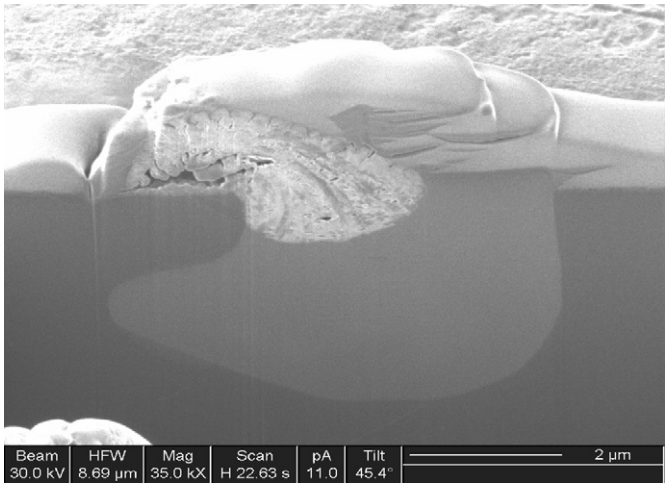

Fig. 9. Secondary electron images of a FIB cut section through a water-reacted carbide inclusion showing consumption of the carbide through hydrous growth formation. The reaction front is clearly visible.

The TEM-determined composition of the hydrated product was found to correlate well with supplementary SIMS data, which recorded a significant concentration of positive UOH^+ ion clusters from the growth phases that was not recorded from the metal or un-reacted carbide inclusions (Fig. 11).

3.2. Water-sample interactions – water purity and gas effects

Repeated experiments carried out in the ESEM, using water of different purity (deionised versus distilled/HPLC), showed an apparent difference in the rate of carbide attack and metaschoepite growth, with the water of higher purity displaying more rapid reaction with the surface carbides.

Additionally, in some ESEM experiments the vapour exposure was deliberately halted (often overnight) by removal of the water vapour using vacuum pumping. During these dormant periods atmospheric gases were allowed to enter the chamber at very low pressures (~5 torr) to assist with sample imaging. Compared with samples that experienced uninterrupted H_2O exposure for the duration of their defined reaction period, samples which were 'stop-started' showed apparently slower subsequent reaction of

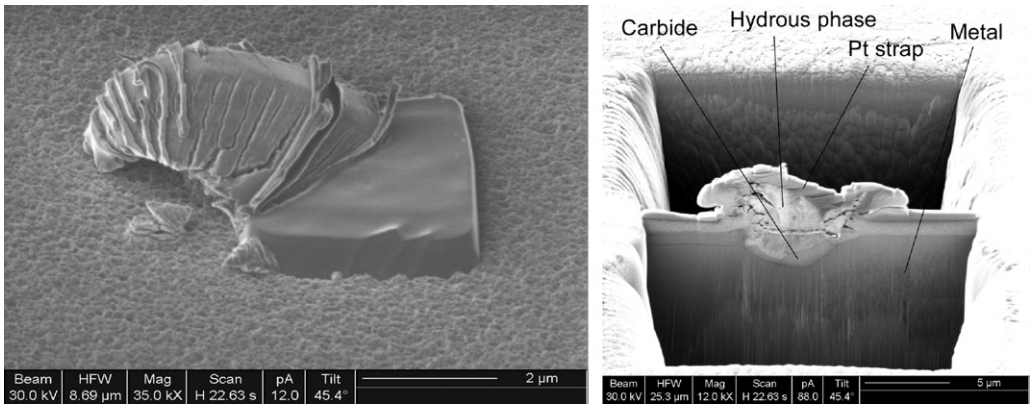

Fig. 10. Secondary electron images of a water-reacted carbide inclusion, before and after preparation for TEM analysis using the FIB system. The section face clearly shows the hydrous growth, carbide inclusion, surrounding metal, surface oxide layer and FIB deposited protective Pt strap.

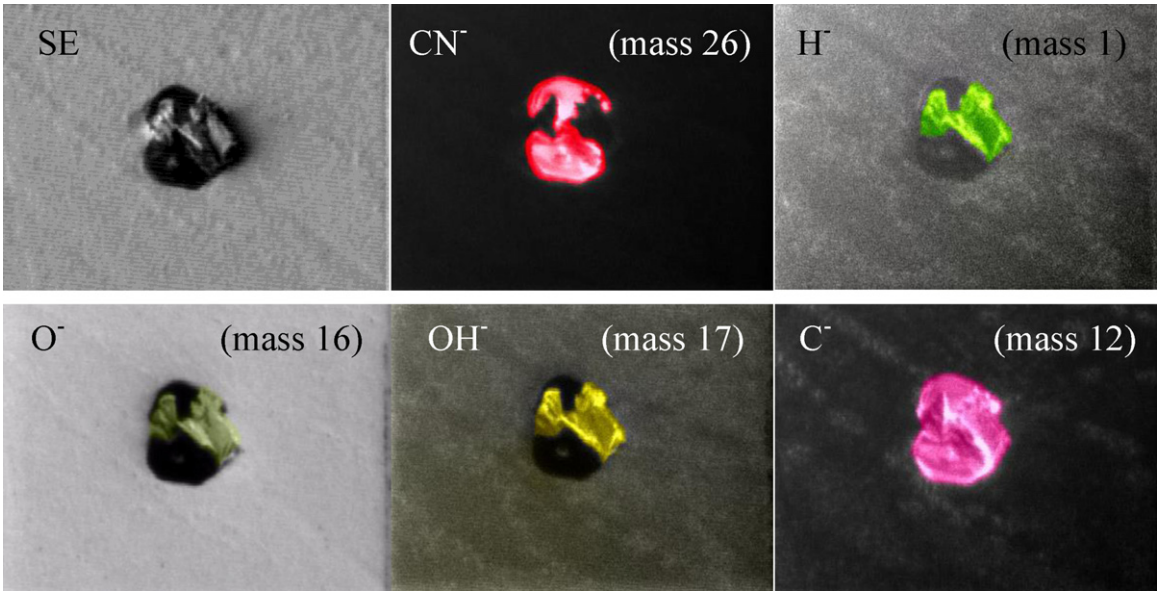

Fig. 11. Negative ion maps recorded for an area of the water-reacted uranium surface, showing the association of different ion clusters with the metal, carbide and metaschoepite growths.

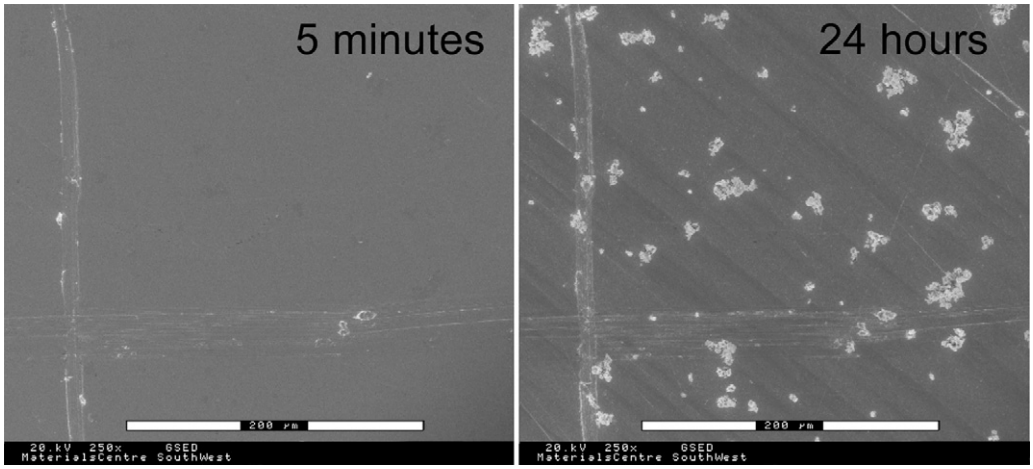

Fig. 12. Secondary electron images of a uranium sample, prepared only by mechanical polishing, before and after exposure to water vapour a 20 mbar and 20 °C in an ESEM system. The image after 24 h exposure clearly shows the development of numerous hydrous growths at carbide inclusions in the metal.

the surface carbides. It is inferred that during dormant periods, atmospheric gas species entering the ESEM chamber would have adsorbed on the sample surface (including carbides) and occupied available sorption sites, subsequently limiting water sorption when the experiment was resumed.

A similar behaviour was observed for water exposure carried out in the gas rig, which showed relatively little reaction of the carbide inclusions on the metal surface when exposed to an H_2O–Ar gas mixture. Although metaschoepite growths were observed, the number recorded was significantly less than would have been expected from a sample grown in the ESEM for the same period. It is not yet clear whether carbide–H_2O decomposition reactions were limited by the presence of the argon (chosen as an inert bystander gas), the overall gas pressure of the system, the free volume of water vapour available or the presence of impurities in the water or argon used for experiment.

3.3. *ESEM water-sample interactions – surface preparation effects*

From the initial tranche of experimental work using electropolished coupons it was not clear if the observed reactivity of the surface carbides was inadvertently related to the electropolishing process, which may have 'activated' the carbide surface in some way. Consequently, to test this theory, further samples were prepared and exposed to water vapour in the ESEM after using only mechanical polishing down to a 4000 grit finish.

The results from analysis by electron microscopy clearly showed similar reactivity of the carbides in the presence of water vapour. Examples of the voluminous metaschoepite growths observed are shown in Figs. 12 and 13 and demonstrate that carbide reactivity is unaffected by preparatory electropolishing of the samples.

4. Discussion

Although the metallic uranium surface was determined to undergo oxidation in the presence of water vapour in the ESEM, the oxidative reaction of the carbide particles, present as impurity phases, was also observed. However, attempts to grow $UO_3{\cdot}H_2O$ on carbide inclusions outside of the ESEM have met with more limited success, attributed to a number of possible factors including water purity, contaminant gases, and overall gas pressure of the reaction system. Further work will be aimed at determining which factors are most significant in limiting carbide decomposition, with the use of isotopic labelling to clarify further the mechanism of $UO_3{\cdot}H_2O$ growth.

Analysis also indicated that the surfaces of the carbide inclusions were covered by a thin film, assumed to be uranium oxide

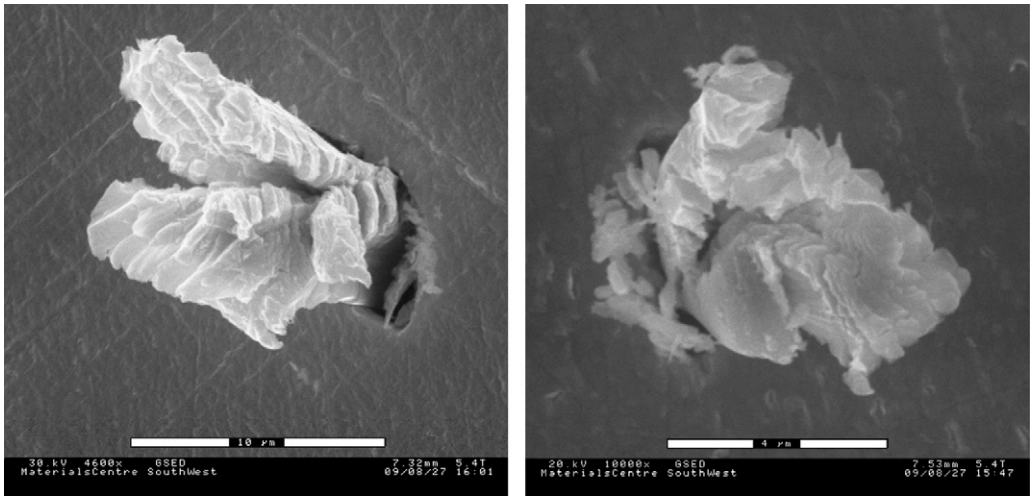

Fig. 13. High resolution secondary electron images of hydrous metaschoepite growths shown in Fig. 12.

(UO_2). The oxide layer (also present on the metal) is thought to have acted as a barrier preventing immediate contact between the water vapour and carbide particles and evidenced by an apparent 'induction' period of a few minutes.

The carbide particles clearly provide zones of chemical impurity in the metal for initiation of corrosion reactions. The observation of $UO_3{\cdot}H_2O$ growths at individual points on the carbide surfaces suggests that oxidative decomposition is energetically favourable in these zones compared to the rest of the exposed particle. Particle corners, edges and boundaries were found to be the primary sites for corrosion initiation. This could be due to disruption of either the inclusion crystal structure or alternatively the inclusion surface oxide layer, resulting in sites of increased susceptibility to oxidative corrosion.

Previously reported reactions of UC and UN with water are given in the equations below [11–15].

$$UC_{(s)} + 2H_2O_{(g)} \rightarrow UO_{2(s)} + C_{(s)} + 2H_{2(g)} \quad (1)$$

$$UC_{(s)} + 2H_2O_{(g)} \rightarrow UO_{2(s)} + CH_{4(g)} \quad (2)$$

$$3UN_{(s)} + 2H_2O_{(g)} \rightarrow UO_{2(s)} + U_2N_{3(s)} + 2H_{2(g)} \quad (3)$$

$$UN_{(s)} + 2H_2O_{(g)} \rightarrow UO_{2(s)} + NH_{3(g)} + 1/2H_{2(g)} \quad (4)$$

These support the detection of various small organic molecules (e.g. acetylene, methane, ethane, ethene, higher order alkenes and alkanes, as well as H_2) highlighted in various reports [2–9,11–21]. However, it should be noted that in the current work the observed growth species is UO_3 based, rather than the UO_2 which is traditionally expected to be formed [11–13,21]. The current result is partly supported by the work of Bradley and Ferris [22], who reported a "gelatinous, hydrous, tetravalent uranium oxide" as the product of bulk UC hydrolysis.

According to Dell et al. [14] UN is much more stable with respect to water than UC, which might provide some explanation for the observed cessation of some metaschoepite growths on carbide particles, related to chemical zoning of the inclusion from UN to UC. Dell's proposed reason for greater stability of UN is the presence of a thin coherent epitaxial film of α-U_2N_3 and super imposed UO_2 at the surface of the nitride which acts to protect the surface from ready reaction. By comparison, a similar film on UC is considered unlikely due to the lack of an intermediate phase for UO_2 to bond to (as UO_2 appears incapable of bonding directly to UC due to the significant difference in lattice parameters).

Based on the data presented in the current work the reactions considered occurring between the carbide particles and water vapour are given in Eqs. (5) and (6).

$$UC_{(s)} + 4H_2O_{(g)} \rightarrow UO_3{\cdot}H_2O_{(s)} + CH4_{(s)} + H_{2(g)} \quad (5)$$

$$2UN_{(s)} + 8H_2O_{(g)} \rightarrow 2UO_3{\cdot}H_2O_{(s)} + 2NH_{3(g)} + 3H_{2(g)} \quad (6)$$

The change in Gibbs free energy for the reactions given in Eqs. (5) and (6) are −431.8 and −462.6 kJ mol^{-1}, respectively. Thus, both of the proposed reactions are concluded to be thermodynamically viable (at 298 K and 1 atm). However, these reactions are not yet considered definitive, and further work using residual gas analysis will be used to determine the gases generated during oxidative decomposition of the carbide inclusions.

Although the rate of reaction of H_2O with the carbo-nitride inclusions has not been empirically assessed separate to the metal, it is possible to make an estimation of the relative rates of reaction. This is undertaken using the experimental observations that some inclusions were completely consumed in 7 days and the surface UO_2 layer present on the surrounding uranium metal thickened by ~880 nm over the same period. In addition, it is observed that the inclusions present in the uranium samples have partitioned zones of UC and UN composition, thus calculations were undertaken assuming inclusion composition of either UC or UN.

A rate of H_2O consumption can be calculated for a hypothetical UC inclusion assuming: (i) an average inclusion diameter of 5 μm, giving an inclusion volume of 125 μm, (ii) the density of UC is 13.63 g cm^{-3}, (iii) reaction proceeds as set out in Eq. (5), (iv) the entire inclusion is consumed in 7 days. This yields a rate of H_2O consumption by UC of 1.80×10^{-10} mol cm^{-2} s^{-1}.

A similar calculation can be carried out for a hypothetical UN inclusion (density = 14.31 g cm^{-3}, volume = 125 μm) being consumed after 7 days by the reaction as set out in Eq. (6). This gives a rate of H_2O consumption by UN of 1.87×10^{-10} mol cm^{-2} s^{-1}.

Using the same approach, the rate of H_2O consumption can be calculated for the uranium metal surface. This is done by assuming the following: that a surface area of 1 μm is considered; the thickness of UO_2 produced after 7 days is 880 nm; the density of UO_2 is 10.97 g cm^{-3} and UO_2 is produced as described in Eq. (7). Thus, a rate of H_2O consumption by the uranium surface of 1.18×10^{-11} mol cm^{-2} s^{-1} is obtained

$$U_{(s)} + 2H_2O_{(g)} \rightarrow UO_2 + 2H_2 \quad (7)$$

It is evident that the estimated rate of H_2O consumption is approximately 15 times faster for decomposition of either a hypothetical UC or UN inclusion, as compared to oxidation of the uranium surface. Thus, it is reasonable to conclude that the experimental rate of H_2O consumption due to reaction with the carbo-nitride inclusions to form $UO_3{\cdot}H_2O$ will be of the order of 15 times faster than the consumption of H_2O due to the formation of UO_2 at the surface of the surrounding uranium.

However, it is vital to determine the relative contributions to the total H_2O consumption of reaction with the inclusions and the surrounding metal. This can be achieved by considering the relative surface areas of inclusion and (UO_2 covered) metal available for reaction with H_2O. If an area of 1 mm^2 is considered, the number of inclusions present at the surface has been determined to be 575. Given an average inclusion diameter of 5 μm, each inclusion has an exposed surface area of 25 μm and the total surface area of inclusions within an area of 1 mm^2 is 0.0144 mm^2, i.e. 1.44% of the surface area.

Therefore, if it is assumed that 100% of the volume of surface inclusions is consumed then the relative rates of H_2O consumption can be calculated for an area of 1 cm^2, using the area specific rates given above and the inclusion/metal surface area ratio of 1.44%. This gives H_2O consumption rates of 2.60×10^{-12} mol s^{-1}, 2.70×10^{-12} mol s^{-1} and 1.17×10^{-11} mol s^{-1} for UC, UN and U, respectively. Assuming that the rates are additive, the contribution from inclusions is ~18% of the total rate.

However, it was observed that not all inclusions underwent total reaction during the course of the experiment, therefore the relative reaction rates must be scaled depending on the proportion of total surface inclusion volume consumed. If it is assumed that the contribution to the H_2O consumption rate for inclusions versus surrounding uranium is directly proportional to the proportion of the available inclusion volume that has reacted, then the calculated contribution from inclusions reduces to 10% for a 50% consumption of surface inclusion volume and 5% for a 25% volume consumption.

In conclusion, the reactions between uranium metal and water have only previously been considered as 'uranium–water', with omnipresent impurity phases either ignored due to their limited abundance or considered as un-reactive bystander species. In the current work the recorded 'inclusion–water' reactions appeared to occur more vigorously than concurrent 'uranium–water' reactions, in actively consuming water vapour. It is therefore likely that reaction results recorded for uranium metals of different purity are very likely to differ, providing a potentially significant source of error. This may partly explain the conflicting data reported by different groups in the literature [1–7].

5. Conclusions

Examination of cast α-uranium surfaces after exposure to water vapour in an ESEM instrument at 19 mbar and 20 °C indicated surface corrosion had occurred, with secondary growths determined to be $UO_3 \cdot H_2O$ (metaschoepite) forming at carbide inclusions across the surface. Over the period of a week the growths were observed to increase in size, consuming only the carbide particles and not the surrounding metal. In some cases complete decomposition of the surface carbides was observed.

From the results of the current study it is apparent that that the carbide particles reacted more readily with the water vapour than the metal. Resultantly it is suggested that disparities between previous studies of the uranium–water reaction may be attributable to differential purities of uranium metal used by different research groups, with resultantly different populations of carbide particles.

References

[1] F. Weigel, Uranium, in: J.J. Katz, G.T. Seaborg, L.R. Morss (Eds.), The Chemistry of the Actinide Elements, Chapman & Hall, London, 1986, p. 245.
[2] J.M. Haschke, Corrosion of uranium in air and water vapor: consequences for environmental dispersal, Journal of Alloys and Compounds 278 (1998) 149–160.
[3] V.S. Yemel'yanov, A.L. Yevstyukhin, The Metallurgy of Nuclear Fuel, Pergamon Press, 1969.
[4] M.M. Baker, L.N. Less, S. Orman, Uranium + water reaction. 1 Kinetics products and mechanism, Transactions of the Faraday Society 62 (1966) 2513–2524.
[5] G.C. Allen, P.M. Tucker, R.A. Lewis, X-ray photoelectron-spectroscopy study of the initial oxidation of uranium metal in oxygen + water-vapor mixtures, Journal of the Chemical Society, Faraday Transactions 2 80 (1984) 991–1000.
[6] A.G. Ritchie, The kinetics and mechanism of the uranium–water vapour reaction – an evaluation of some published work, Journal of Nuclear Materials 120 (1984) 143–153.
[7] G.W. McGillivray, D.A. Geeson, R.C. Greenwood, Studies of the kinetics and mechanism of the oxidation of uranium by dry and moist air: a model for determining the oxidation rate over a wide range of temperatures and water vapour pressures, Journal of Nuclear Materials 208 (1994) 81–97.
[8] B.R.T. Frost, The carbides of uranium, Journal of Nuclear Materials 10 (1963) 265–300.
[9] P.E. Evans, T.J. Davies, Uranium nitrides, Journal of Nuclear Materials 10 (1963) 43–55.
[10] T. Ishitani, H. Tsuboi, T. Yaguchi, H. Koike, Transmission electron microscope sample preparation using a focused ion beam, Journal of Electron Microscopy 43 (1994) 322–326.
[11] R. Asuvathraman, S. Rajagopalan, K. Ananthasivan, C.K. Mathews, R.M. Mallya, Surface studies on uranium monocarbide using XPS and SIMS, Journal of Nuclear Materials 224 (1995) 25–30.
[12] Y. Hori, T. Mukaibo, Kinetic studies of the reaction between uranium monocarbide and water vapour, Bulletin of the Chemical Society of Japan 40 (1967) 1878–1883.
[13] A. Schürenkämper, Kinetic studies of the hydrolysis of uranium monocarbide in the temperature range 30–90 °C, Journal of Inorganic and Nuclear Chemistry 32 (1970) 417–429.
[14] R.M. Dell, V.J. Wheeler, N.J. Bridger, Hydrolysis of uranium mononitride, Transactions of the Faraday Society 63 (1967) 1286–1294.
[15] G.A.R. Rao, S.K. Mukerjee, V.N. Vaidya, V. Venugopal, D.D. Sood, Oxidation and Hydrolysis kinetic-studies on UN, Journal of Nuclear Materials 185 (1991) 231–241.
[16] L.J. Colby Jr., Kinetics of the reaction of uranium monocarbide with water, Journal of the Less Common Metals 10 (1966) 425–431.
[17] C.P. Kempter, Hydrolysis properties of uranium monocarbide and dicarbide, Journal of the Less Common Metals 4 (1962) 419–425.
[18] M.J. Bradley, L.M. Ferris, Hydrolysis of uranium carbides between 25 and 100°. III. Uranium sesquicarbide and mixtures of the sesquicarbide with monocarbide or dicarbide, Inorganic Chemistry 3 (1964) 730–734.
[19] M.J. Bradley, L.M. Ferris, Hydrolysis of uranium carbides between 25 and 100°. II. Uranium dicarbide, uranium metal-monocarbide mixtures, and uranium monocarbide-dicarbide mixtures, Inorganic Chemistry 3 (1964) 189–195.
[20] M.I. Ermolaev, G.V. Tishchenko, Reaction of uranium monocarbide with acid and alkaline solutions, Izvestija vysšich učebnych zavedenij, Khim. Khim. Tekhnol. 16 (11) (1973) 1631–1633.
[21] B. Hájek, P. Karen, V. Brožek, Hydrolysis of uranium monocarbide, Collection of Czechoslovak Chemical Communications 49 (1984) 793–804.
[22] M.J. Bradley, L.M. Ferris, Hydrolysis of uranium carbides between 25 and 100°. I. Uranium monocarbide, Inorganic Chemistry 1 (1962) 683–687.